ELSEVIER

Integrin-αvβ6 targeted peptide-toxin therapy in a novel αvβ6-expressing immunocompetent model of pancreatic cancer

Nicholas F. Brown [a, 1], Elizabeth R. Murray [a, 1], Lauren C. Cutmore [a, 1], Philip Howard [b], Luke Masterson [b], Francesca Zammarchi [c], John A. Hartley [d], Patrick H. van Berkel [c], John F. Marshall [a, *]

[a] *Centre for Tumour Biology, Barts Cancer Institute, Queen Mary University of London, John Vane Science Centre, Charterhouse Square, London, EC1M 6BQ, UK*
[b] *Spirogen, QMB Innovation Centre, 42 New Road, London, E1 2AX, UK*
[c] *ADC Therapeutics (UK) Ltd, Translation & Innovation Hub Building, Imperial College White City Campus, 84 Wood Lane, London, W12 0BZ, UK*
[d] *Cancer Research UK Drug-DNA Interactions Research Group, University College London Cancer Institute, 72 Huntley Street, London, WC1E 6BT, UK*

ARTICLE INFO

ABSTRACT

Previously we reported that a novel αvβ6-specific peptide-drug conjugate (SG3299) could eliminate established human pancreatic ductal adenocarcinoma (PDAC) xenografts. However the development of effective therapies for PDAC, which is an essential need, must show efficacy in relevant immunocompetent animals. Previously we reported that the KPC mouse transgenic PDAC model that closely recapitulates most stages of development of human PDAC, unlike in humans, failed to express αvβ6 on their tumours or metastases. In this study we have taken the KPC-derived PDAC line TB32043 and engineered a variant line (TB32043mb6S2) that expresses mouse integrin αvβ6. We report that orthotopic implantation of the αvβ6 over-expressing TB32043mb6S2 cells promotes shorter overall survival and increase in metastases. Moreover, systemic treatment of mice with established TB32043mb6S2 tumours in the pancreas with SG2399 lived significantly longer (p < 0.001; mean OS 48d) compared with PBS or control SG3511 (mean OS 25.5d and 26d, respectively). Thus SG3299 is confirmed as a promising candidate therapeutic for the therapy of PDAC.

1. Introduction

Pancreatic ductal adenocarcinoma (PDAC) is the third most common cause of cancer death [1]. The majority of patients (~80%) have metastatic disease at presentation, most commonly in the liver (80%), peritoneum (69%), lungs (50−70%), and adrenal glands (25%) [2]. Prognosis is poor, with 1 and 5 year survival rates of 25% and 7% respectively [3]. Combination cytotoxic chemotherapies are the mainstay of treatment for metastatic disease [4,5]. Despite the introduction of novel chemotherapy regimens, there has been no improvement in long term survival since the 1970s [3], and more effective therapies are urgently needed.

The integrin αvβ6 is expressed on ~85% of pancreatic cancers with minimal expression in healthy tissues, and thus is a valid therapeutic target [6−11]. We previously developed the A20FMDV2 peptide that binds with high-affinity to αvβ6 [12]. SG3299 is a peptide-toxin conjugate that conjugates A20FMDV2 to a synthetic pyrrolobenzodiazepine (PBD) dimer cytotoxic warhead with a cathepsin B-cleavable valine-alanine linker. We have shown that SG3299 is highly effective in subcutaneous pancreatic cancer xenografts in immunodeficient models, with prolonged survival and tumour eliminations [13].

However, these models do not recapitulate the PDAC tumour microenvironment (TME) that is considered a major barrier to effective therapies. The TME accounts for 40−90% of tumour bulk, half of which are immune cells that produce a profoundly immunosuppressive and fibrotic TME [14−18]. Human xenografts require immunodeficient mice that cannot faithfully recreate the TME and murine cell-line xenografts within immune-competent mice generate a "vaccine effect" with immune activation and an atypical TME [19−21]. Heterotopic xenografts (typically subcutaneous) rarely metastasise and their outputs are rarely reproducible in clinical studies [22]. The KPC (LSL-Kras^{G12D}; LSL-Trp53^{R172H};Pdx-1-

---

* Corresponding author.
E-mail address: j.f.marshall@qmul.ac.uk (J.F. Marshall).
[1] These authors contributed equally.

N.F. Brown, E.R. Murray, L.C. Cutmore et al.

Cre) PDAC immunocompetent mouse PDAC model overcomes these limitations, with highly desmoplastic tumours comprising an immunosuppressive TME, metastases, and clinical features that mimic that of PDAC including resistance to therapies [20,23–28].

In this manuscript, we describe the development of an αvβ6-expressing orthotopic PDAC model in immunocompetent mice and demonstrate the effectiveness of the αvβ6-targeted peptide toxin SG3299 in this system.

2. Methods

2.1. Cell culture

Murine PDAC tumour derived cell cultures were from KPC: TB13381, TB32043, TB32047, R254L, Claus (a gift from Claus Jorgenson, Manchester, UK); KPF (LSL-Kras$^{G12D/+}$;LSL-p53$^{R172H/+}$;Pdx-Flp): TB32048; and KC (LSL-Kras^{G12D};Pdx-1-Cre) (DT6066, a gift from from Dave Tuveson, Cold Spring Harbor Laboratory, USA) mice. Murine PDAC cells were grown as adherent monolayers in DMEM supplemented with 10% FBS in 5% (vol/vol) of CO_2/air at 37 °C.

2.2. Flow cytometry

Murine PDAC cells were dissociated with TrypleE Express (12604013, ThermoFisher) and washed three times with ice cold DMEM 0.1%/0.1% buffer (0.1% (w/v) bovine serum albumin (BSA) (A7906, Sigma Aldrich)/0.1% (w/v) sodium azide (NaN$_3$) (S8032, Sigma Aldrich)). Cells were incubated with 1 μl of anti- αvβ6 antibody (clone 10D5) (MAB2077Z, Millipore) for 1 h at 4 °C. The cells were washed again with cold DMEM 0.1%/0.1% buffer and incubated with Alexa Fluor 488−conjugated goat anti-mouse secondary antibody (10337882, ThermoFisher) antibody at a 1:200 dilution for 30 min at 4 °C in the dark. Following one final wash with cold DMEM 0.1%/0.1% buffer, cells were resuspended in FACS buffer (DMEM 0.1%/0.1% buffer and 0.5 μg/mL DAPI 1:5000 (62248, ThermoFisher)) and analysed by flow cytometry on a BD LSR Fortessa (BD Biosciences).

A series of fluorochrome-labelled variants of A20FMDV2 were synthesised by Peptide Protein Research 284 Ltd. (Cambridge, United Kingdom): Cy3-A20FMDV2 and Cy5- A20FMDV2 were produced by conjugating Cy3 or Cy5 directly to the N-terminus of the A20FMDV2 peptide (NK(biotinyl)VPNLRGDLQVLAQKVART). A separate scrambled peptide (NK(biotinyl)LRDQTGLKNPVQLARVAV) with an N-terminal Cy3 was also created (previously described by Meecham et al., 2022 [29]). For flow cytometry analysis samples were prepared as above and cells were incubated with 100 nM of peptide.

2.3. In-vitro cell proliferation assays

Mitochondrial activity, as a surrogate measure for cell viability, was measured using WST-1 assay. Cells were seeded at 3x10^3 cells/mL in a 96-well plate in triplicate. After 24 h the cells were treated with 0−105 nM of αvβ6-targeted SG3299 or non-targeted SG3511 peptide drug conjugate. After 48 h the cells were used in WST-1 assay. Media was removed from cells and 200 μl of Proliferation Reagent WST-1 (5015944001, Merck) (diluted 1:10) was added to the wells. After 2 h the absorbance of the wells was measured at 450 nm with a reference wavelength of 650 nm, using a colorimetric plate reader (InfiniteF50, Tecan).

2.4. Immunofluorescence staining

1.8X10^4 cells were seeded onto 13 mm coverslips overnight. The following day cells were washed three times with cold PBS and fixed with 4% paraformaldehyde for 10 min. Cells were washed three times in PBS before blocking for 30 min with DMEM 0.1%/0.1% buffer. Primary antibody was diluted 1:100 in blocking buffer and cells were incubated at RT for 1 h. Following three washes with DMEM 0.1%/0.1% buffer the cells were permeabilized for 10 min with 0.1% Triton X-100 in blocking buffer. Cells were then incubated with anti-mouse IgG Alexa Fluor-488 (A11029, Invitrogen) secondary antibody diluted 1:500 for 30 min at room temperature. Cells were counterstained with Rhodamine Phalloidin (R415, Invitrogen) (1:1000) and DAPI (62248, ThemoFisher) (1:5000). Coverslips were washed and mounted onto slides using ProLong Gold Antifade mountant (P36934, ThermoFisher). Cells were visualized using LSM710 confocal microscope (Zeiss).

2.5. Western blotting

3 x 10^5 cells were seeded in 6-well plates. After 48 h the cells were washed 3X with ice cold PBS, and lysed with 200 μl sample buffer (3% SDS, 60 mM sucrose, 65 mM Tris pH 6.8). Lysates were homogenized by passing through a 27G needle followed by centrifugation at 13,000 RPM for 3 min. Protein concentration was determined using the DC™ Protein Assay Kit (5000111, Bio-Rad) following the manufacturer's guidelines. 10 μg of protein was loaded into a 10% mini-SDS-PAGE gel and the gel was run at 80 V for 30 min followed by 90 min at 120 V. Resolved proteins were transferred to a nitrocellulose membrane (Amersham Hybond TM ECLTM RPN303D, GE Healthcare©) using wet transfer overnight at 12V. Non-specific binding was blocked by incubating membrane in 3% BSA TBST for 30 min at room temperature. The blots were probed with primary antibody overnight at 4 °C. αvβ6 was detected using goat anti-β6 C-19 diluted in 3% BSA TBST +0.1% NaN$_3$ (sc-6632, Santa Cruz)((1:1000). Secondary anti-goat HRP was incubated with the blot for 1 h at room temperature (P0160, Dako) (1:2000).

2.6. Cloning and virus production

A gene fragment (gBlock) encoding murine β6 (uniprot Q9Z0T9) was synthesised by IDT (Integrated DNA Technologies, Belgium). The fragment was cloned into the pWPXL vector using restriction digest cloning. pWPXL was a gift from Didier Trono (Addgene plasmid # 12257). The correct insertion of the sequence was confirmed by Sanger sequencing.

Lentiviral particles were produced via transfection of the lentiviral constructs into HEK293T human embryonic kidney cells. 24 hrs after seeding, cells were transfected with VSV.G (Addgene, 14888), Pax2 (Addgene, 35002), and WPXL-mb6 plasmids using Lipofectamine 2000 Transfection Reagent (11668030, ThermoFisher). 48 and 72 h supernatants were collected, pooled and ultracentrifuged (23,000×g, 2 h, 4 °C). The concentrated virus, supplemented with polybrene 4 μg/mL (H9268, Sigma Aldrich), was added to an adherent monolayer of TB32043 cells at approximately 80% confluency.

Firefly luciferase-expressing cells were established by transducing cells with a PGK-GFP-IRES-Luciferase Lentivector system from Addgene. Cells expressing firefly luciferase were sorted for by selecting cells with GFP expression with a FACS BD Aria II instrument (BD) and subsequently expanded in vitro.

2.7. Orthotopic murine tumor models

All *in vivo* experiments were performed in accordance with the guidelines issued by the UK Home Office under approved Project Licenses. C57BL/6J mice (approximately 12 weeks old) were pre-medicated with 100 μL buprenorphine (30 μg/mL) intraperitoneally (57133-02, Vetergesic; Ceva) and anaesthetised with isofluorane (10015516, Zoetis). An incision was made in the skin on the left axillary line, 5 mm below the costal margin. A 7–8 mm incision was made in the peritoneum and the spleen was mobilised extracorporeally. 1000 TB32043 or TB32043mb6s2 cells mixed with 10 μL of Matrigel (354234, Corning) to a volume of 30 μL were injected into the pancreas using an insulin syringe (0.3 ml MicroFine, 324826, BD). The pancreas and spleen were returned to the abdominal cavity, the peritoneum closed with absorbable sutures (C0022002, Braun), and the skin with wound clips (726063, Harvard Apparatus). Wound clips were removed one week after surgery. Mice were terminated following UK Home Office regulations or when the Humane Endpoints (HE) had been reached.

2.8. Magnetic resonance imaging

MRI's were performed on a Bruker ICON™ 1T MRI system (Bruker). Mice were anaesthetised with isoflurane. Images were acquired using Rapid Imaging with Refocused Echoes spiral T2-weighted (T2-RARE) sequences, with signal acquisition gated to respiration. MR Images were analysed in VivoQuant v3.5 (InviCRO). Tumour volume was measured by adding manually delineated regions of interest (ROIs) for each MR slice. Where multiple tumours were visible, the volume of the largest primary tumour was measured.

2.9. In-vivo bioluminescence imaging

Mice received 150 mg/kg luciferin (P1043, Promega) intraperitoneally 10 min before image acquisition. Hair was shaved from the torso of the mice and they were anaesthetised with isoflurane. Bioluminescent images were acquired using an *in vivo* imaging system (IVIS) (Lumina III with ZFOV-24 Lens, PerkinElmer) for 10 s, 30 s, and using the "Auto" setting with medium and small binning. Images were analysed with Living Image (Caliper Life Sciences). A rectangular region of interest was used to delineate mice and luciferase activity was reported as photons per second ($p/s/cm^2/sr$).

2.10. Peptide-toxin administration

Peptide-Toxins SG3299 and SG3511 were generated by Spirogen (QMB Innovations, London) using modified A20FMDV2 peptides synthesised by Peptide Protein Research Ltd (Hampshire, UK; >95% purity). Thus A20FMDV2 was modified by addition of an N-terminal biotin and a C-terminal cysteine. SG3249 (tesirine), composed of a cathepsin B-cleavable valine-alanine linker conjugated to a synthetic pyrrolobenzodiazepine dimer SG3199 [30], was conjugated to the C terminus of the peptide to create the αvβ6 targeting peptide-toxin conjugate SG3299. A non-targeting peptide scrambled was conjugated to the same cytotoxic payload SG3249 to create the control SG3511, as previously described by Moore et al., 2020 [31]. Mice received 136 μg/kg of SG3299 or SG3511 (equivalent to 20 μg/kg SG3199) intraperitoneally in 200 μl PBS twice a week for two weeks. Mice in the PBS control group were given 200 μl of intraperitoneal PBS.

3. Immunohistochemistry

Tumours and tissues of interest were immediately post-mortem placed in 10% formalin (BAF-0010-01A, Cellstor) for 24-h, placed in 70% ethanol, and then paraffin embedded. Tumour sections were stained for CD3 (A0452, Dako), endomucin (SC-53941 V.5C7, Santa Cruz), Ki67 (15580, Abcam), cleave caspase 3 (9664, Cell Signaling Technology)(1:2000), and sirius red (F3B, C.I.35782). Staining was performed using the discovery XT automated IHC research slide staining system. Staining for αvβ6 was performed manually as described previously [32]. Slides were scanned using Pannoramic 250 High Flash III (3DHISTECH) and images were viewed in Pannoramic Viewer v1.15.4 (3DHISTECH).

Visiopharm Image Analysis Software (Visopharm) was used to quantify tissue staining and immunohistochemistry. The Tissue Detection application (Visopharm) was used to delineate tissue from background. Non-tumour tissue was manually delineated and removed from the ROI. Visiopharm applications (APPs) for respective morphological and immunohistochemistry stains (designed in-house) were used to quantify the positive staining within the ROIs.

3.1. Statistical analysis

Statistical analysis was performed using GraphPad Prism (Systat Software, USA). Error bars in all experiments represent standard deviation (SD) in in vitro studies and standard error of the mean (SEM). For 2 variables, data were analysed using an unpaired-two-tailed student t-test (unless otherwise stated). For 3 or more variables data were analysed using one-way ANOVA with Tukey's multiple comparisons test. Individual tumour growth curves were plotted and differences between treatments were tested using simple linear regression analysis. IC_{50} values were calculated using non-linear regression analysis with sum-of-squares F test. The statistical analyses used in each experiment is detailed in the figure legend. In in vivo experiments, n refers to the number of animals. In in vitro experiments, n refers to the number of biological replicates.

4. Results

4.1. Development of an KPC-derived αvβ6-expressing PDAC tumour model

The integrin αvβ6 expression was evaluated by flow cytometry using antibody 10D5 on cell cultures derived from 8 PDAC tumours from immunocompetent murine transgenic models, including KPC (LSL-Kras$_{G12D}$; LSL-Trp53$_{R172H}$;Pdx-1-Cre), KC (LSL-Kras^{G12D};Pdx-1-Cre), and KPF (LSL-Kras$^{G12D/+}$;LSL-p53$^{R172H/+}$;Pdx-Flp) mice. αvβ6 expression was absent to moderate in all cell lines tested (Fig. 1A), comprehensively lower than that seen in human PDAC samples [11,31]. The KPC derived culture TB32043 was selected as a consistent minimal expresser of αvβ6 via flow cytometry (4.4 ± 2.9%) (Fig. 1A). TB32043 cells were transduced with pWPXL-mb6 lentivirus, and were FACS sorted twice to select for the highest αvβ6 expressers, the resultant cells termed TB32043mb6s2 (Fig. S1). The KPC origin of TB32043mb6s2 was confirmed by genotyping (Transnetyx, Inc; USA) with Kras-G12D ± and TP53++ mutations present. TB32043mb6s2 consistently expressed αvβ6, even with prolonged culture (Fig. 1B and S1).

Immunofluorescence staining on adherent cells confirmed surface expression of αvβ6 on TB32043mb6s2 cells, with no visible αvβ6 on TB32043 cells (Fig. 1C). αvβ6 expression caused a morphological change in the TB32043 cells, causing a more mesenchymal appearance with marked lamellipodia. Western blotting similarly confirmed the presence of β6 within TB32043mb6s2 cells, with no detectable αvβ6 in TB32043 (Fig. 1D). Thus the apparent 'minimal' αvβ6 expression on TB32043 cells detected by flow cytometry is likely to be an artefact due to cytometry gating as both western blotting and immunofluorescence confirm these cells are αvβ6-negative.
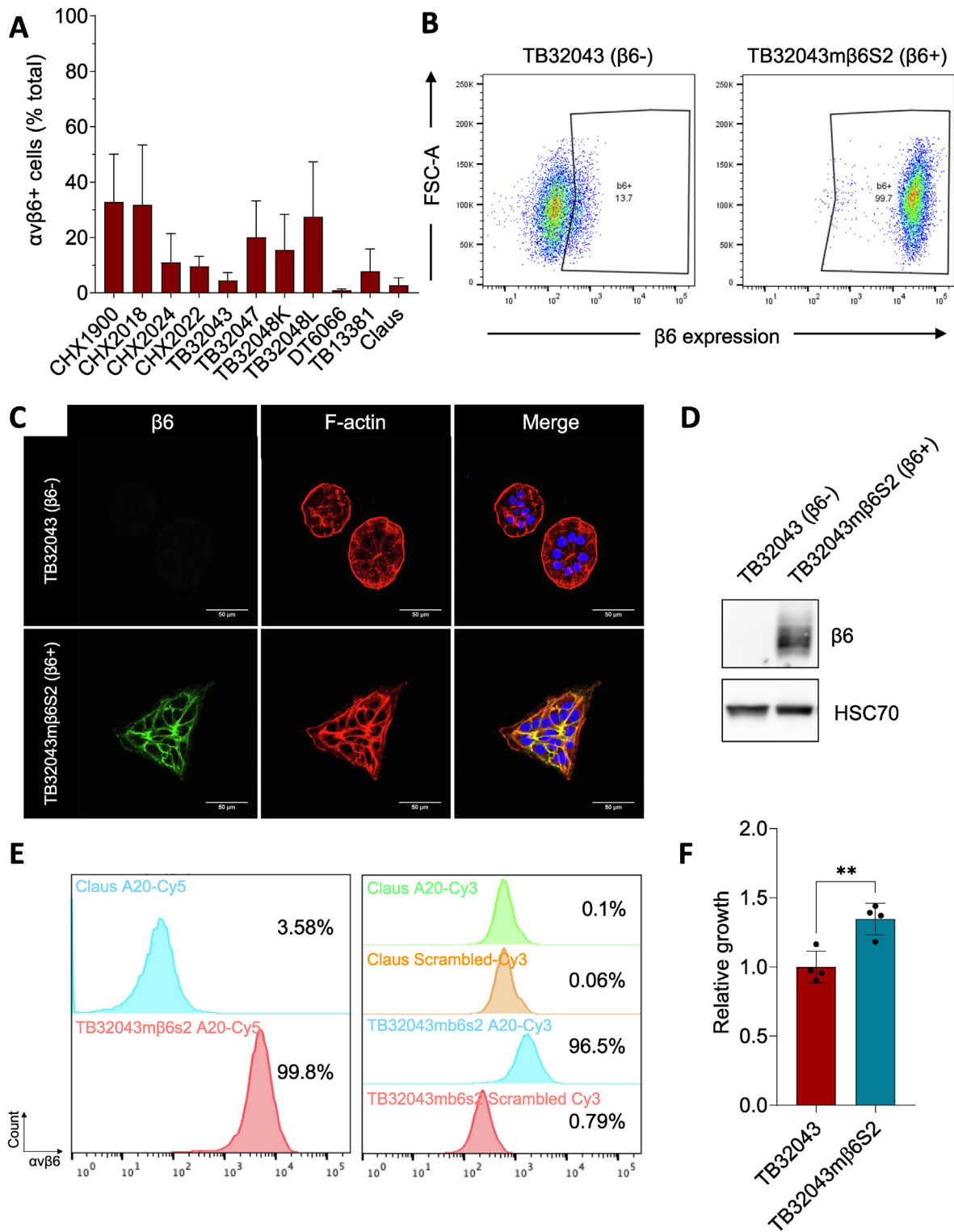
Fig. 1. Development of a KPC-derived PDAC tumour cell model expressing αvβ6. (A) αvβ6 expression on a panel of murine KPC-derived PDAC cell lines by flow cytometry (mean ± SD, n = 2−9 samples/condition). (B−D) Expression of αvβ6 in the parental β6-negative TB32043 cell line and β6-positive TB32043mβ6S2 cell line by flow cytometry (B), immunofluorescence (C) and Western blot (D). Scale bar 50 μm. Data representative of at least 3 biological replicates. (E) Binding of Cy3/Cy5-A20MDV2 or Cy3/Cy5-scrambled peptide to TB32043mβ6s2 (β6+) and Claus (β6-) cells. (F) Relative growth rate of TB32043mβ6S2 cells relative to TB32043 cells in 2D culture (n = 4 biological replicates, unpaired *t*-test).

The functionality of the murine αvβ6 expressed on TB32043mb6s2 was evaluated by assessing the binding of fluorophore conjugated-A20FMDV2 peptides using flow cytometry. The control peptide used the same amino-acids as A20FMDV2 but was scrambled. A20FMDV2-Cy3 bound to 96.5% of TB32043mb6s2 cells compared to 0.59% binding with the control-Cy3 peptide.
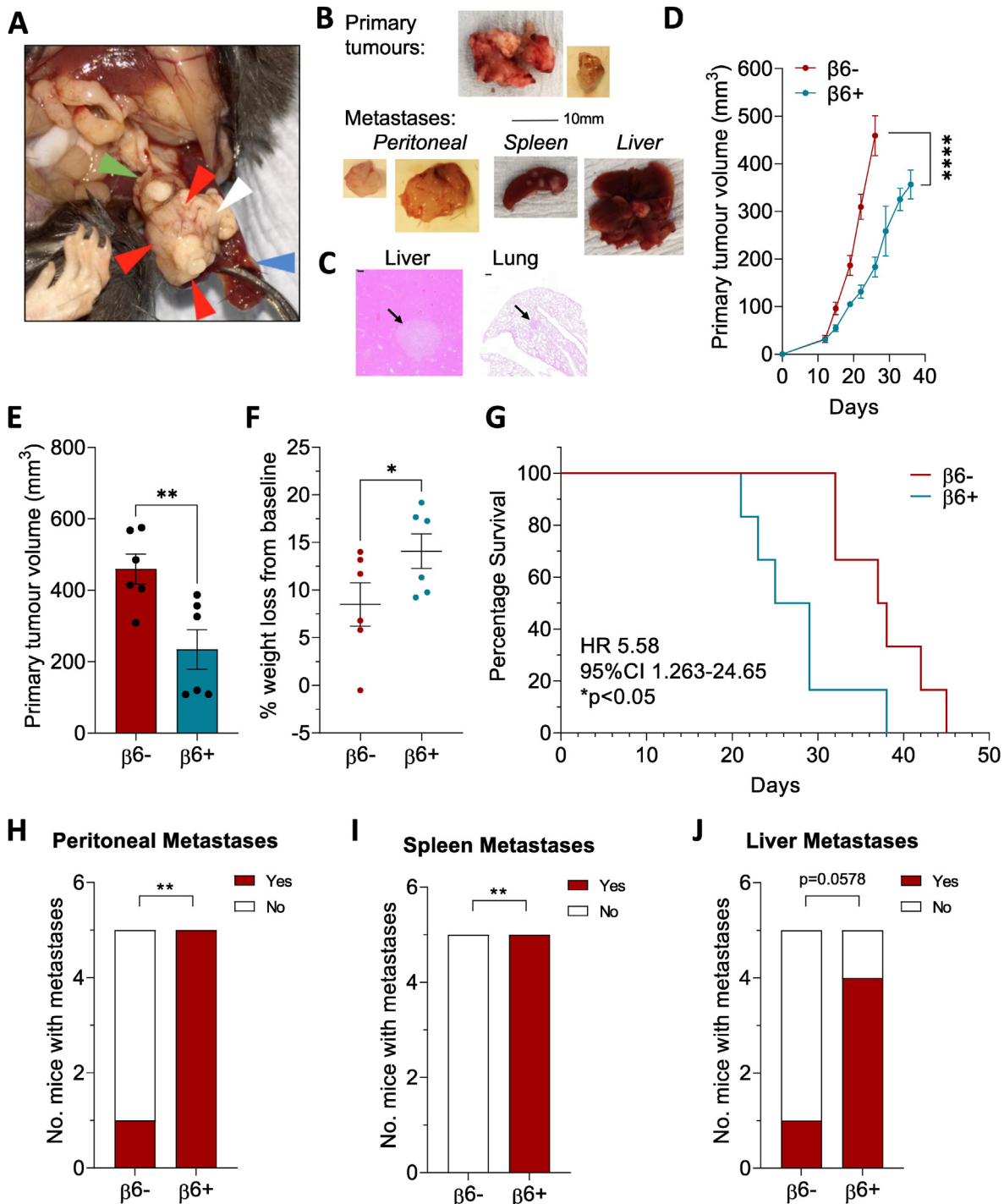
N.F. Brown, E.R. Murray, L.C. Cutmore et al.

Fig. 2. αvβ6 expression reduces survival and increases spontaneous metastases of mice with pancreatic tumours. (A) Orthotopic injection of PDAC cells into the pancreas results in the formation of solid pancreatic tumours with spontaneous metastases, shown in a representative mouse. Red arrows: tumour; white: pancreas; blue: spleen lesion: green: small intestine adherent to tumour. (B) Dissected primary tumours, peritoneal tumours, spleen metastases, and liver porta hepatis tumour shown as indicated. (C) H&E staining of metastases within liver and lung sections (scale bars represent 200 μm) (D) Primary tumour volume determined by MRI in mice injected with TB32043 cells (β6-) or TB32043mβ6S2 cells (β6+) (n = 6 mice/condition, p < 0.0001, simple linear regression analysis). (E) Primary tumour volume at death of mice injected with β6-or β6+ PDAC cells (n = 6 mice/condition). (F) Maximum weight loss of mice injected orthotopically with β6-or β6+ PDAC cells (mean ± SEM, n = 6 mice/condition, representative of 3 biological experiments). (G) Mice injected with β6-positive PDAC cells have a significantly shorter survival relative to mice injected with β6-negative PDAC cells (n = 6 mice/condition, p < 0.05, logrank Mantel-Cox test). (H–J) αvβ6 expression enhances the spontaneous metastasis of pancreatic tumours to the peritoneum (H), spleen (I) and liver (J) when injected orthotopically into C57BL/6 mice (n = 5 mice/group, p < 0.01, Chi-square test). Statistical significance is indicated by asterisks; * for p < 0.05, ** for p < 0.01, **** for p < 0.001.

Binding to αvβ6-weak-expressing cells was minimal with 0.1% and 0.06% binding seen with A20FMDV2-Cy3 or scrambled-Cy3 respectively (Fig. 1E). αvβ6 expression caused a significant increase in the relative growth rate of TB32043mb6s2 compared to the parental αvβ6 negative line in vitro (1.346 vs 1.000, p = 0.005) (Fig. 1F).
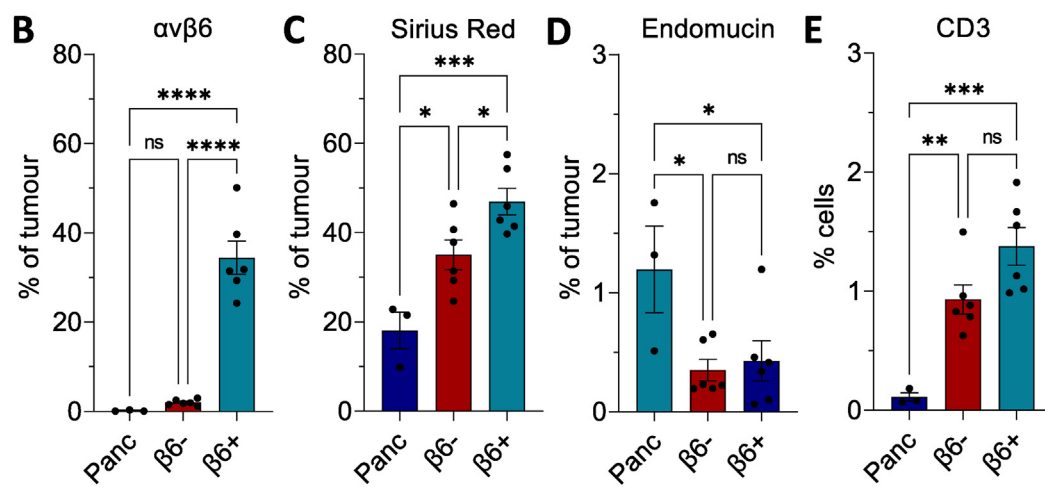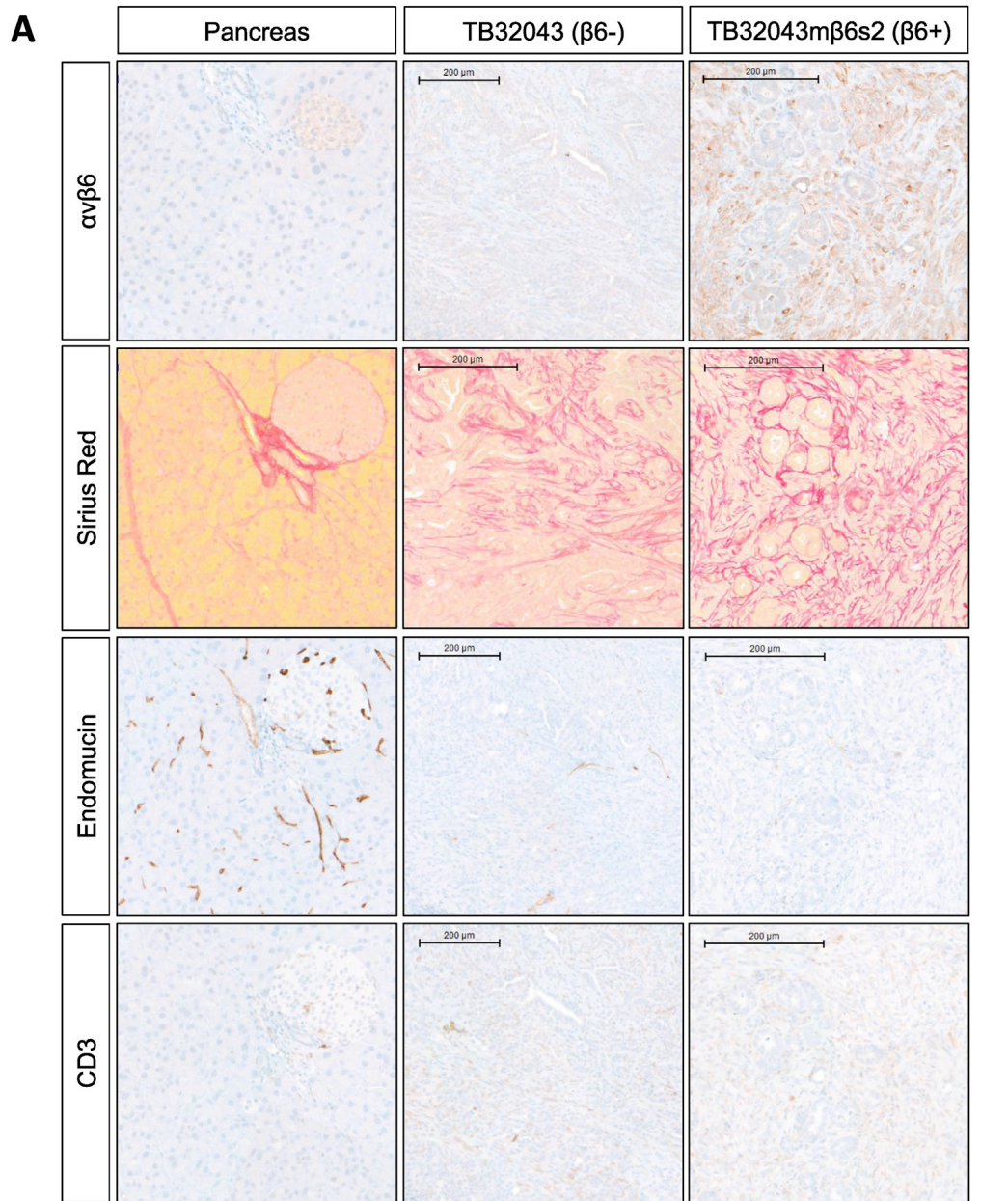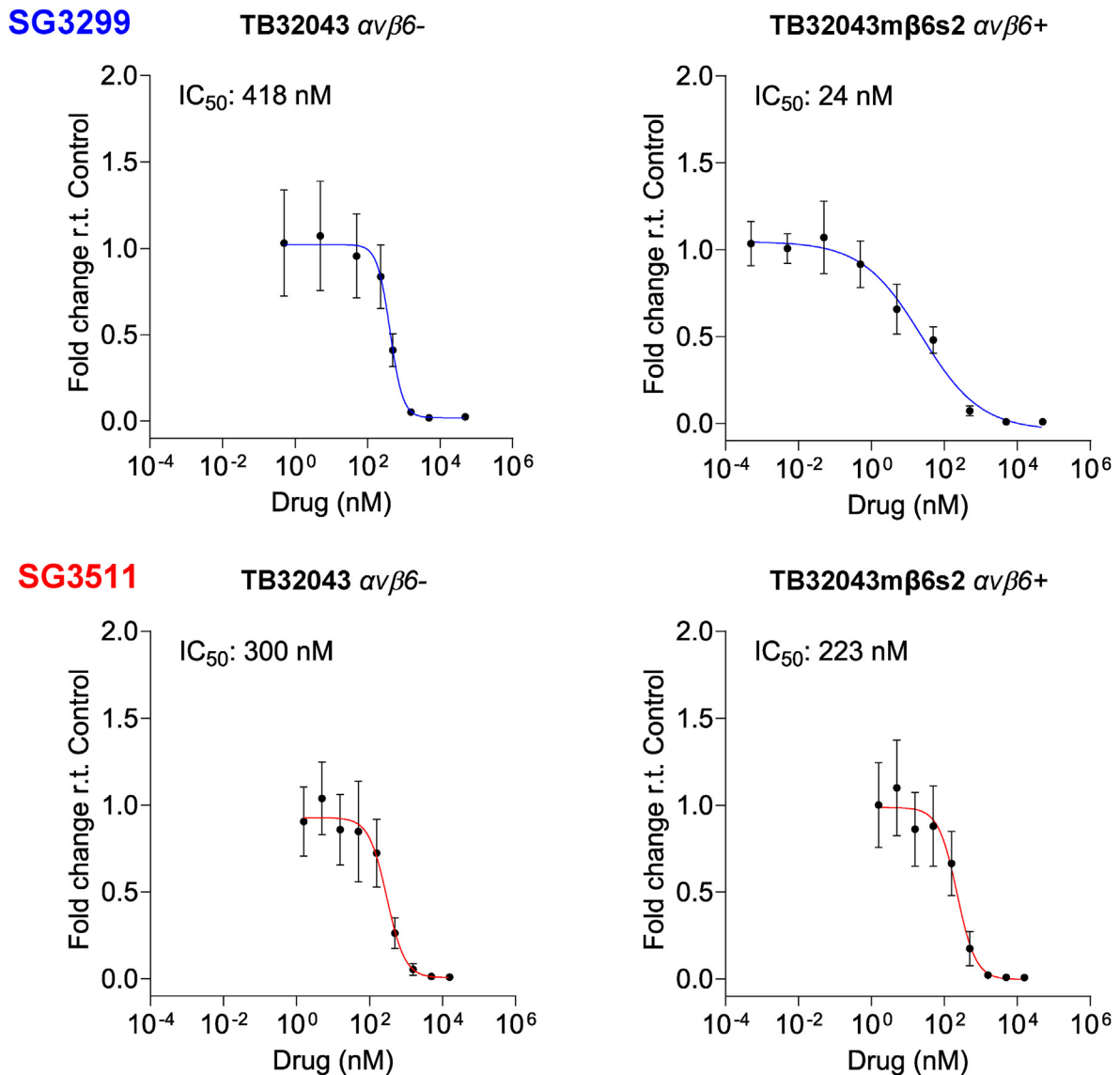
Fig. 4. Efficacy of β6-targeted SG3299 therapy *in vitro*. (A) Cytotoxic efficacy of the αvβ6-targeting SG3299 or non-targeting SG3511 peptide drug conjugates against β6- TB32043 cells or β6+ TB32043mβs2 cells. Graphs show fold change relative to untreated cells (B) Summary of IC50 data. Each value is mean ± SD, n = 3 biological repeats for SG3511, n = 2 biological replicates for SG3299; each comprises 3 technical repeats. P < 0.0001, non-linear regression analysis with sum-of-squares F test.

4.2. αvβ6 expression reduces survival and increases metastases of mice with pancreatic tumours

In vivo, orthotopic injection of TB32043mb6s2 cells into the pancreas of C57BL/6J mice resulted in the formation of dense primary pancreatic tumours as well as metastasis on the peritoneum, spleen and liver (Fig. 2A–C). The rate of tumour volume increase in mice injected with the αvβ6-expressing TB32043mb6s2 cells was significantly lower than those injected with the αvβ6-negative parental TB32043 cells (Fig. 2D; p < 0.0001), with a significantly lower final volume (234.4 vs 459.3 mm^3, p = 0.0089) (Fig. 2E). However, despite a smaller tumour burden, TB32043mb6s2 mice experienced significantly greater weight loss (14.1% vs 8.5%,

p = 0.0418) (Fig. 2F) and significantly shorter survival (median survival 27 vs 37.5 days, p = 0.0223) compared to TB32043 mice (Fig. 2G). Additionally, a higher proportion of mice injected with TB32043mb6s2 developed metastases in the spleen (100 vs 0%, p < 0.01), peritoneum (100 vs 20%, p < 0.01), and liver (80 vs 20% p = 0.058) (Fig. 2H–J).

4.3. αvβ6 expressing pancreatic ductal adenocarcinomas have distinct histology

Both TB32043 and TB32043mb6s2 derived tumours were generally poorly differentiated with areas of differentiated glandular tissue and central necrosis (data not shown). As expected

Fig. 3. β6 expression promotes the formation of poorly vascularised tumours with increased collagen desmoplasia. (A) Representative sections of healthy pancreas (n = 3), β6-TB32043-derived tumours (n = 6) and β6+ TB32043mβs2-derived tumours (n = 6) stained for αvβ6, sirius red, endomucin and CD3. (B–E) Quantification of positively stained tumour area for αvβ6 (B), sirius red (C), endomucin (D) and CD3 (E). Mean ± SEM, *p < 0.05, **p < 0.01, ***p < 0.001, ****p < 0.0001, one-way ANOVA with Tukey's multiple comparisons test.
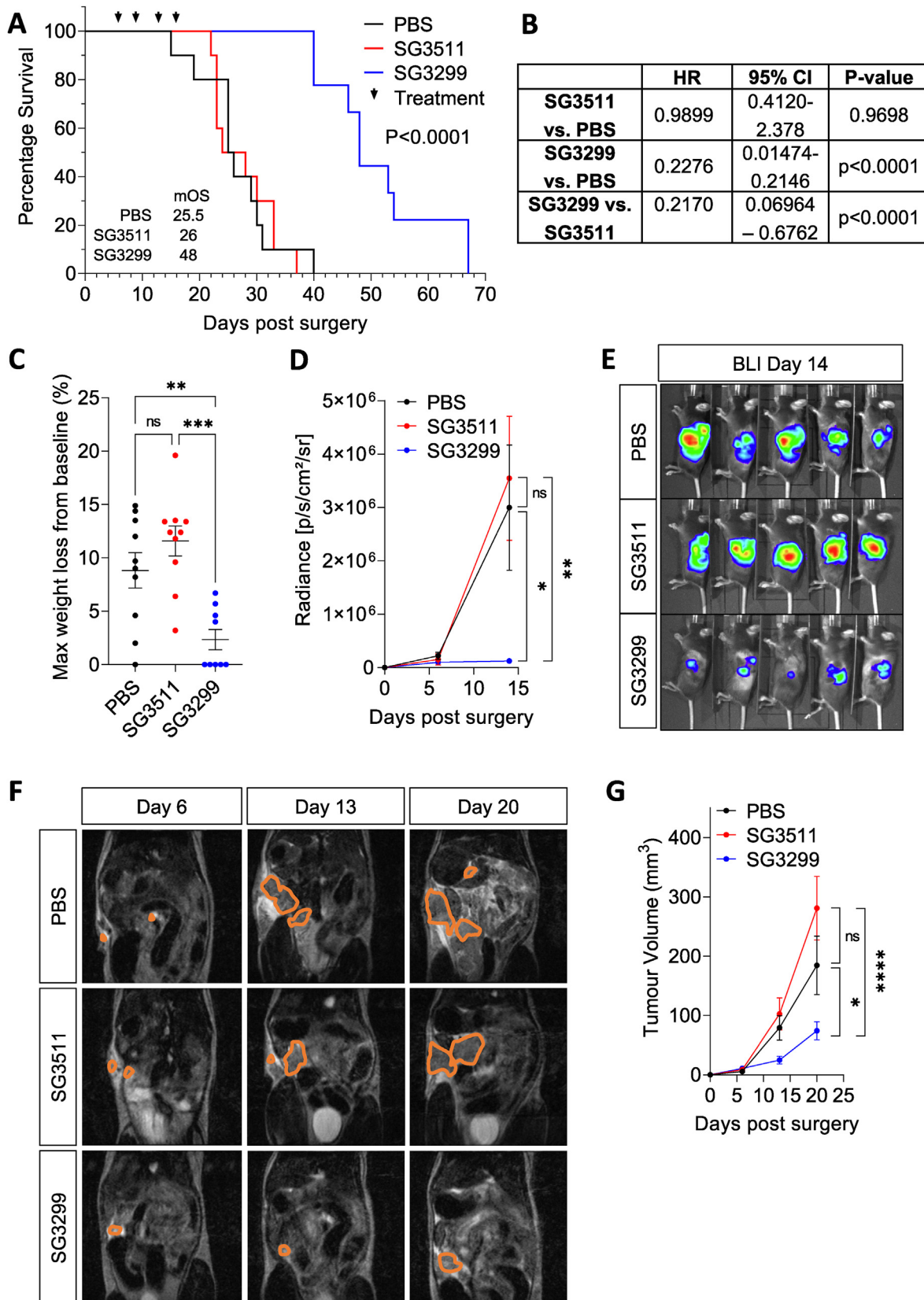
N.F. Brown, E.R. Murray, L.C. Cutmore et al.

Fig. 5. αvβ6-targeting peptide-drug conjugate SG3299 significantly increases survival and reduces tumour burden of immunocompetent mice with αvβ6-positive pancreatic tumours. (A) Kaplan Meier survival curve of mice injected orthotopically with TB32043mβ6s2 cells and treated with SG3299, SG3511 or PBS after 7 days (n = 8−9 mice/group, p < 0.001, logrank Mantel-Cox test). Median overall survival (mOS) displayed in days in inset. (B) Hazard ratio (HR), 95% confidence interval (CI) and statistical significance between PBS, SG3511 and SG3299 treatment groups (n = 8−9 mice/group, repeated logrank Mantel-Cox test with Bonferroni correction). (C) Maximum weight loss of mice treated with PBS, SG3511 or SG3299 (mean ± SEM, n = 8−9 mice/group, **p < 0.01, ***p < 0.001, one-way ANOVA with Tukey's multiple comparisons test). (D) Tumour burden of

N.F. Brown, E.R. Murray, L.C. Cutmore et al.

αvβ6 expression was higher in TB32043mb6s2 tumours than TB32043 tumours and normal pancreas (34 vs 2 vs 0% respectively, p < 0.0001) (Fig. 3A and B). TB3204mb6s2 tumours contained significantly more collagen than TB32043 tumours (47 vs 35%, p = 0.0461) and normal pancreas (47% vs 18%, p = 0.0005) (Fig. 3C). TB32043 and TB32043mb6s2 were both hypovascular relative to normal pancreas (0.35 vs 0.43 vs 1.2%, p < 0.05) and contained higher numbers of T-cells (0.93% vs 1.38% vs 0.11%, p < 0.01) (Fig. 3D and E).

4.4. SG3299 has αvβ6-specific cytotoxicity against murine PDAC cells in vitro

In previous studies our group identified a high-affinity 20 amino-acid sequence NAVPNLRGDLQVLAQKVART (termed A20FMDV2) that binds specifically to integrin αvβ6, and subsequently developed an A20FMDV2 based peptide-drug conjugate [13,33,34]. SG3299 is composed of A20FMDV2 peptide with an N-terminal biotin and a C-terminal cysteine conjugated to the cytotoxic payload tesirine (SG3249). Tesirine is composed of a cathepsin B-cleavable linker and the PBD dimer cytotoxic warhead SG3199 [30]. The toxin prevents cell replication by covalently cross-linking DNA in the minor groove. A non-targeting scrambled peptide was also conjugated to the toxic payload to create a control, SG3511. We sought to test the cytotoxic activity of SG3299 in our αvβ6-expressing immunocompetent model of PDAC.

The relative specificity of SG3299 for αvβ6, and the in vitro cytotoxic effect of SG3299 on αvβ6-expressing murine cancer cells was confirmed with a growth inhibition assay performed on TB32043mb6s2 and TB32043 cells (high & negative αvβ6 expression respectively). Cell viability was evaluated with a WST-1 assay following treatment with 0−105 nM of SG3299 or SG3511. The IC$_{50}$ of αvβ6-targeted SG3299 in TB32043mb6s2 was over 15-fold lower than in TB32043 cells (24 nM vs 418 nM, p < 0.001) (Fig. 4A and B). There was no significant difference in the IC50 values for the non-targeted SG3511 between TB32043mb6s2 and TB32043 cells (223 vs 300 nM, p = 0.17) (Fig. 4).

4.5. SG3299 improves survival and reduces tumour burden in an in vivo immunocompetent orthotopic metastatic αvβ6-expressing PDAC model

Seven days after orthotopic injection of TB32043mb6s2 cells, when tumours were visible by bioluminescence, mice were treated with PBS, SG3299 or SG3511 at doses equivalent to 20 μg/kg of the payload. Median survival was significantly longer in mice treated with the αvβ6-targeted SG3299 (48 days) compared to those treated with non-targeting SG3511 (26 days, HR 0.22 95% CI 0.070−0.68, p < 0.0001) or PBS (25.5 days, HR 0.23, 95% CI 0.015−0.21, p < 0.0001) (Fig. 5A and B). Mice treated with SG3299 experienced significantly less total body weight loss (2.33%) than those treated with SG3511 (11.57%, p = 0.0082) or PBS (8.83%, p = 0.0002) (Fig. 5C). Tumour burden was assessed by MRI volume and IVIS bioluminescence quantification (Fig. 5C−G). There was no significant difference in pre-treatment tumour burden by IVIS (p = 0.57) nor MRI (p = 0.13). Following treatment, bioluminescence was significantly lower in mice treated with SG3299 than SG3511 (p = 0.0037) and PBS (p = 0.0178), and tumour volume

assessed by MRI was lower in the SG3299 group than SG3511 (p < 0.001) and PBS (p < 0.05) groups. Using an ELISA assay specific for the payload (described previously [13]) a pharmacokinetic study demonstrated that intraperitoneal administration of SG3299 led to rapid absorption into blood with a peak concentration seen at 15 min of 69.5+/111.8 nM, the concentration remaining above 60 nM for 2h, before complete elimination by 4 h (Fig. S2).

5. Discussion

More effective therapies are desperately needed for patients with pancreatic cancer. Patient studies confirm integrin αvβ6 as a potential target for therapy [6−11], and we have previously demonstrated the therapeutic efficacy of targeting αvβ6 in vivo [11,13]. This study describes for the first time the creation of an immunocompetent murine PDAC model that expresses αvβ6, thereby more closely mimicking human PDAC tumours. We show, that the peptide-drug conjugate SG3299 remains an effective therapeutic in this immunocompetent PDAC model.

This study affords new insights into how αvβ6-expression may alter PDAC behaviour. In vitro, αvβ6-expression increased cell growth, yet in vivo αvβ6-expressing tumours grew more slowly but led to greater weight loss and shorter survival, with more collagenous tumours that metastasised more readily. This is consistent with human PDAC where αvβ6-expression is associated with poorer survival [9,11]. Whilst increased proliferation in vitro with higher αvβ6-expression is documented [35,36], reduce tumour size in vivo was not predicted. αvβ6-expression appeared to result in significant loss of body weight (Fig. 2F), which is a prominent feature of human pancreatic cancer. It would be premature to suggest that αvβ6 promotes cancer-associated cachexia which is a complex metabolic phenomenon of which TGFβ is a key mediator [37] even though αvβ6 can induce TGFβ activation [38−40], as we cannot exclude that our observations could have resulted from αvβ6-induced local pancreatic invasion, reducing pancreatic enzyme secretion, and limiting nutrient absorption.

This study in our immunocompetent orthotopic PDAC murine model supports previous studies in heterotopic immunodeficient PDAC models that the αvβ6-targeted peptide-toxin SG3299 is tolerable, reduces tumour growth, and improves survival. It is worth noting that in vitro our KPC-derived cells appear relatively resistant to SG3299 therapy when compared to human cell lines, with IC50 of 24 nM vs 0.06 and 0.55 nM in Colo357 and PancO43 human PDAC cell lines respectively, despite similarly high αvβ6-expression [13]. The broadly similar αvβ6-specificity ratios (ratio of IC50 value for SG3511/SG3299) of 18 with TB32043mb6s2 versus 10.97 for Colo357 and 13.22 for Panc0403 [13] suggests the treatment resistance is inherent to the TB32043 KPC derived cells, rather than a feature of ectopic αvβ6 expression.

Our previous studies with SG3299 in heterotopic immunodeficient PDAC models have found tumour eradication and cure with established Capan-1 xenografts, and tumour regression but not eradication in Panc04.03 + PS1 pancreatic stellate cell xenografts. However, we did not observe any tumour regressions in our immunocompetent model. Thus whilst SG3299 has demonstrated efficacy in all assessed PDAC models, it appears to be less effective as the tumour exceeds a certain size and/or the tumour microenvironment becomes increasingly rich and established, supporting

mice treated with PBS, SG3511 or SG3299 assessed by bioluminescence imaging (BLI) (mean ± SEM, n = 8−9 mice/group, *p < 0.05, **p < 0.01, two-way ANOVA with Tukey's multiple comparisons test. (E) Representative BLI pictures of mice treated with PBS, SG3511 or SG3299 taken o Day 14 post-surgery. (F) Representative MRI images of mice treated with PBS, SG3511 or SG3299. Tumours are delineated in orange. Mice displayed had the median tumour size in their respective treatment groups on Day 20 (n = 5 mice/group). (G) Tumour volume of mice treated with PBS, SG3511 or SG3299 assessed by MRI (mean ± SEM, n = 5 mice/group, *p < 0.05, ****p < 0.0001, two-way ANOVA with Tukey's multiple comparisons test.

future combination studies with anti-stromal agents.

There is a stark disparity between the effectiveness of anticancer therapies in preclinical models and patients. Only 2.3% of pancreatic cancer therapies tested in phase I trials are eventually approved for clinical use [41]. It is therefore reasonable to deduce that the PDAC models used in the majority of prior preclinical studies (typically heterotopic xenografts in immunodeficient animals) do not sufficiently recapitulate the human disease to predict response or resistance to therapy. Given the vast majority of human PDAC tumours express αvβ6, and the immune-component is a key element of the tumour micro-environment, we believe it is important that these components are included in any model evaluating therapies for PDAC, whether the therapies are targeting αvβ6 or not.

Acknowledgement

Please not that no AI tool was used in any part of this manuscript.

Appendix A. Supplementary data

Supplementary data to this article can be found online at https://doi.org/10.1016/j.pan.2024.02.013.

References

[1] Siegel RL, Miller KD, Jemal A. "Cancer statistics. CA A Cancer J Clin 2017;67(1): 7—30. https://doi.org/10.3322/caac.21387. Jan 2017.

[2] Winter JM, Maitra A, Yeo CJ. "Genetics and pathology of pancreatic cancer,". HPB : the official journal of the International Hepato Pancreato Biliary Association 2006;8(5):324—36. https://doi.org/10.1080/13651820600804203.

[3] Cancer Research Uk. Pancreatic cancer statistics. http://www.cancerresearchuk.org/health-professional/cancer-statistics/statistics-by-cancer-type/pancreatic-cancer. [Accessed 30 March 2018].

[4] National Institute for Health and Care Excellence. Pancreatic cancer in adults: diagnosis and management. NICE Guideline NG85; 2018.

[5] Ducreux M, et al. Cancer of the pancreas: ESMO Clinical Practice Guidelines for diagnosis, treatment and follow-upeng, editor. Ann Oncol Sep 2015;26(Suppl 5):v56—68. https://doi.org/10.1093/annonc/mdv295.

[6] Sipos B, et al. Immunohistochemical screening for β6-integrin subunit expression in adenocarcinomas using a novel monoclonal antibody reveals strong up-regulation in pancreatic ductal adenocarcinomas in vivo and in vitro. Histopathology 2004;45(3):226—36. https://doi.org/10.1111/j.1365-2559.2004.01919.x.

[7] Tummers WS, et al. Selection of optimal molecular targets for tumor-specific imaging in pancreatic ductal adenocarcinomaeng, editor. Oncotarget Aug 22 2017;8(34):56816—28. https://doi.org/10.18632/oncotarget.18232.

[8] de Geus SW, et al. Selecting tumor-specific molecular targets in pancreatic adenocarcinoma: paving the way for image-guided pancreatic surgery. In: Molecular imaging and biology : mib : the official publication of the Academy of Molecular Imaging, 18; Dec 2016. p. 807—19. https://doi.org/10.1007/s11307-016-0959-4. 6.

[9] Li Z, et al. Integrin β6 acts as an unfavorable prognostic indicator and promotes cellular malignant behaviors via ERK-ETS1 pathway in pancreatic ductal adenocarcinoma (PDAC). Tumor Biol 2016/04/01 2016;37(4):5117—31. https://doi.org/10.1007/s13277-015-4353-7.

[10] Vallath SS. Studying the role of integrin αVβ6 in pancreatic cancer. In: Doctoral Thesis. Queen Mary University of London; 2013 [Online]. Available: https://ethos.bl.uk/OrderDetails.do?did=1&uin=uk.bl.ethos.667175.

[11] Reader CS, et al. The integrin alphavbeta6 drives pancreatic cancer through diverse mechanisms and represents an effective target for therapy. J Pathol Nov 2019;249(3):332—42. https://doi.org/10.1002/path.5320.

[12] DiCara D, et al. Structure-function analysis of Arg-Gly-Asp helix motifs in alpha v beta 6 integrin ligands. J Biol Chem 2007;282(13):9657—65. https://doi.org/10.1074/jbc.M610461200.

[13] Moore K, et al. Integrin αvβ6-specific therapy for pancreatic cancer developed

[14] from foot-and-mouth-disease virus. Theranostics 2020;10(7):2930—42.

[14] Olive KP. Stroma, stroma everywhere (far more than you think). Clin Cancer Res 2015;21(15):3366—8. https://doi.org/10.1158/1078-0432.ccr-15-0416.

[15] Makohon-Moore AP, et al. Limited heterogeneity of known driver gene mutations among the metastases of individual patients with pancreatic cancer. online Nat Genet 2017;49:358. https://doi.org/10.1038/ng.3764. https://www.nature.com/articles/ng.3764#supplementary-information.

[16] Torphy RJ, et al. Stromal content is correlated with tissue site, contrast retention, and survival in pancreatic adenocarcinoma. JCO Precis Oncol 2018;10:1200. https://doi.org/10.1200/PO.17.00121. PO.17.00121, 2018.

[17] Mahadevan D, Von Hoff DD. Tumor-stroma interactions in pancreatic ductal adenocarcinoma. Mol Cancer Therapeut 2007;6(4):1186—97. https://doi.org/10.1158/1535-7163.mct-06-0686.

[18] Clark CE, Hingorani SR, Mick R, Combs C, Tuveson DA, Vonderheide RH. Dynamics of the immune reaction to pancreatic cancer from inception to invasion. Cancer Res 2007;67(19):9518—27. https://doi.org/10.1158/0008-5472.can-07-0175.

[19] Beatty GL, Paterson Y. IFN-gamma can promote tumor evasion of the immune system in vivo by down-regulating cellular levels of an endogenous tumor antigen. 10. In: Journal of immunology (Baltimore, Md), 165; 1950. p. 5502—8. Nov 15 2000.

[20] J. W. Lee, C. A. Komar, F. Bengsch, K. Graham, and G. L. Beatty, "Genetically engineered mouse models of pancreatic cancer: the KPC model (LSL-Kras(G12D/+);LSL-Trp53(R172H/+);Pdx-1-Cre), its variants and their application in immuno-oncology drug discovery," Current protocols in pharmacology/editorial board, S.J. Enna *(editor-in-chief). [*et al.], vol. 73, pp. 14.39.1-14.39.20, 06/01 2016, doi: 10.1002/cpph.2.

[21] Adunka T. Characterization of murine pancreatic carcinoma models regarding immunosuppressive mechanisms and therapy with bifunctional siRNA targeting galectin-1. In: Doctorate in human biology, department of clinical pharmacology, ludwig maximilian university of Munich ludwig maximilian university of Munich library; 2014 [Online]. Available: https://edoc.ub.uni-muenchen.de/17449/1/Adunka_Tina.pdf.

[22] Herreros-Villanueva M, Hijona E, Cosme A, Bujanda L. Mouse models of pancreatic cancer. World J Gastroenterol Mar 28 2012;18(12):1286—94. https://doi.org/10.3748/wjg.v18.i12.1286.

[23] Beatty GL, et al. "CD40 agonists alter tumor stroma and show efficacy against pancreatic carcinoma in mice and humans". Science (New York, NY) Mar 25 2011;331(6024):1612—6. https://doi.org/10.1126/science.1198443.

[24] Feig C, et al. "Targeting CXCL12 from FAP-expressing carcinoma-associated fibroblasts synergizes with anti-PD-L1 immunotherapy in pancreatic cancer". Proc Natl Acad Sci USA Dec 10 2013;110(50):20212—7. https://doi.org/10.1073/pnas.1320318110.

[25] Hingorani SR, et al. Trp53R172H and KrasG12D cooperate to promote chromosomal instability and widely metastatic pancreatic ductal adenocarcinoma in miceeng, editor. Cancer Cell May 2005;7(5):469—83. https://doi.org/10.1016/j.ccr.2005.04.023.

[26] Jacobetz MA, et al. Hyaluronan impairs vascular function and drug delivery in a mouse model of pancreatic cancer. Gut Jan 2013;62(1):112—20. https://doi.org/10.1136/gutjnl-2012-302529.

[27] Olive KP, et al. Inhibition of Hedgehog signaling enhances delivery of chemotherapy in a mouse model of pancreatic cancereng, editor. Science (New York, NY) Jun 12 2009;324(5933):1457—61. https://doi.org/10.1126/science.1171362.

[28] Provenzano PP, Cuevas C, Chang AE, Goel VK, Von Hoff DD, Hingorani SR. Enzymatic targeting of the stroma ablates physical barriers to treatment of pancreatic ductal adenocarcinomaeng, editor. Cancer Cell Mar 20 2012;21(3): 418—29. https://doi.org/10.1016/j.ccr.2012.01.007.

[29] Meecham A, Cutmore LC, Protopapa P, Rigby LG, Marshall JF. Ligand-bound integrin αvβ6 internalisation and trafficking. Front Cell Dev Biol 2022;10: 920303. https://doi.org/10.3389/fcell.2022.920303.

[30] Hartley JA, et al. Pre-clinical pharmacology and mechanism of action of SG3199, the pyrrolobenzodiazepine (PBD) dimer warhead component of antibody-drug conjugate (ADC) payload tesirine. Sci Rep Jul 11 2018;8(1): 10479. https://doi.org/10.1038/s41598-018-28533-4.

[31] Moore KM, et al. Integrin αvβ6-specific therapy for pancreatic cancer developed from foot-and-mouth-disease viruseng, editor. Theranostics 2020;10(7): 2930—42. https://doi.org/10.7150/thno.38702.

[32] Moore KM, et al. Therapeutic targeting of integrin alphavbeta6 in breast cancer. J Natl Cancer Inst Aug 2014;106(8). https://doi.org/10.1093/jnci/dju169.

[33] DiCara D, et al. Structure-function analysis of Arg-Gly-Asp helix motifs in alpha v beta 6 integrin ligands. The Journal of biological chemistry 2007;282(13):9657—65. https://doi.org/10.1074/jbc.M610461200. Mar 30.

[34] Meecham A, Marshall J. Harnessing the power of foot-and-mouth-disease virus for targeting integrin alpha-v beta-6 for the therapy of cancer. Expet Opin Drug Discov Jul 2021;16(7):737—44. https://doi.org/10.1080/17460441.2021.1878143.

[35] Agrez M, Chen A, Cone RI, Pytela R, Sheppard D. The alpha v beta 6 integrin promotes proliferation of colon carcinoma cells through a unique region of the beta 6 cytoplasmic domain. J Cell Biol Oct 1994;127(2):547—56. https://doi.org/10.1083/jcb.127.2.547.

[36] Ahmed N, et al. Direct integrin alphavbeta6-ERK binding: implications for tumour growth. Oncogene, Original Paper Feb 21 2002;21(9):1370—80. https://doi.org/10.1038/sj.onc.1205286.

[37] Baracos VE, Martin L, Korc M, Guttridge DC, Fearon KCH. Cancer-associated cachexia. Nat Rev Dis Prim 2018;4:17105. https://doi.org/10.1038/nrdp.2017.105. 01.

[38] Munger JS, et al. The integrin alpha v beta 6 binds and activates latent TGF beta 1: a mechanism for regulating pulmonary inflammation and fibrosis. Cell Feb 5 1999;96(3):319−28.

[39] Shi M, et al. Latent TGF-beta structure and activation. Nature Jun 15 2011;474(7351):343−9. https://doi.org/10.1038/nature10152.

[40] Dong X, Hudson NE, Lu C, Springer TA. Structural determinants of integrin beta-subunit specificity for latent TGF-beta. Nat Struct Mol Biol Dec 2014;21(12):1091−6. https://doi.org/10.1038/nsmb.2905.

[41] Hay M, Thomas DW, Craighead JL, Economides C, Rosenthal J. Clinical development success rates for investigational drugs. Nat Biotechnol Jan 2014;32(1):40−51. https://doi.org/10.1038/nbt.2786.